Star Formation Quenching in Green Valley Galaxies at $0.5 \lesssim z \lesssim 1.0$ and Constraints with Galaxy Morphologies

J. P. Nogueira-Cavalcante,[1,2⋆] T. S. Gonçalves,[1] K. Menéndez-Delmestre,[1] and K. Sheth[3,4]

[1] *Observatório do Valongo, Universidade Federal of Rio de Janeiro, Ladeira Pedro Antônio, 43, Saúde 20080-090, Rio de Janeiro, Brazil*
[2] *Observatório Nacional, Rua Gal. José Cristino 77, São Cristóvão 20921-400 Rio de Janeiro RJ, Brazil*
[3] *National Radio Astronomy Observatory, 520 Edgemont Road, Charlottesville, VA 22903, USA*
[4] *NASA HQ, 300 E Street SW, Washington DC 20546, USA*

arXiv:1709.07015v1 [astro-ph.GA] 20 Sep 2017

Accepted XXX. Received YYY; in original form ZZZ

ABSTRACT

We calculate the star formation quenching timescales in green valley galaxies at intermediate redshifts ($z \sim 0.5 - 1$) using stacked zCOSMOS spectra of different galaxy morphological types: spheroidal, disk-like, irregular and merger, dividing disk-like galaxies further into unbarred, weakly-barred and strongly-barred, assuming a simple exponentially-decaying star formation history model and based on the H_δ absorption feature and the 4000 Å break. We find that different morphological types present different star formation quenching timescales, reinforcing the idea that the galaxy morphology is strongly correlated with the physical processes responsible for quenching star formation. Our quantification of the star formation quenching timescale indicates that disks have typical timescales 60% to 5 times longer than that of galaxies presenting spheroidal, irregular or merger morphologies. Barred galaxies in particular present the slowest transition timescales through the green valley. This suggests that although secular evolution may ultimately lead to gas exhaustion in the host galaxy via bar-induced gas inflows that trigger star formation activity, secular agents are not major contributors in the rapid quenching of galaxies at these redshifts. Galaxy interaction, associated with the elliptical, irregular and merger morphologies contribute, to a more significant degree, to the fast transition through the green valley at these redshifts. In the light of previous works suggesting that both secular and merger processes are responsible for the star formation quenching at low redshifts, our results provide an explanation to the recent findings that star formation quenching happened at a faster pace at $z \sim 0.8$.

Key words: galaxies: evolution – galaxies: high-redshift – galaxies: structure – galaxies: stellar content – galaxies: star formation

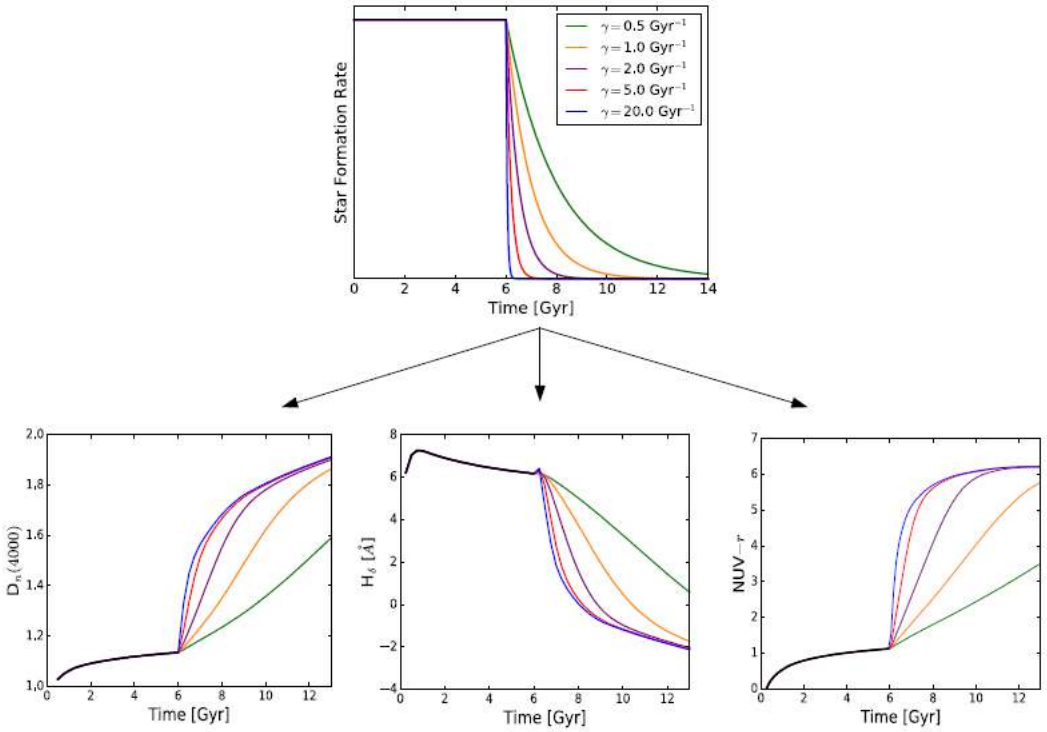

Figure 1. ***Top***: Star formation rate as a function of time for five different SFHs with exponential decay (equations 1 and 2). ***Bott*** $D_n(4000)$ and $H_{\delta A}$ indices and NUV$-r$ colour as functions of time, assuming the exponentially-decaying SFHs with different γ ind shown on the top panel. The faster the star formation quenching (i.e., higher γ value) is, the sharper the time variation of these ind will be.

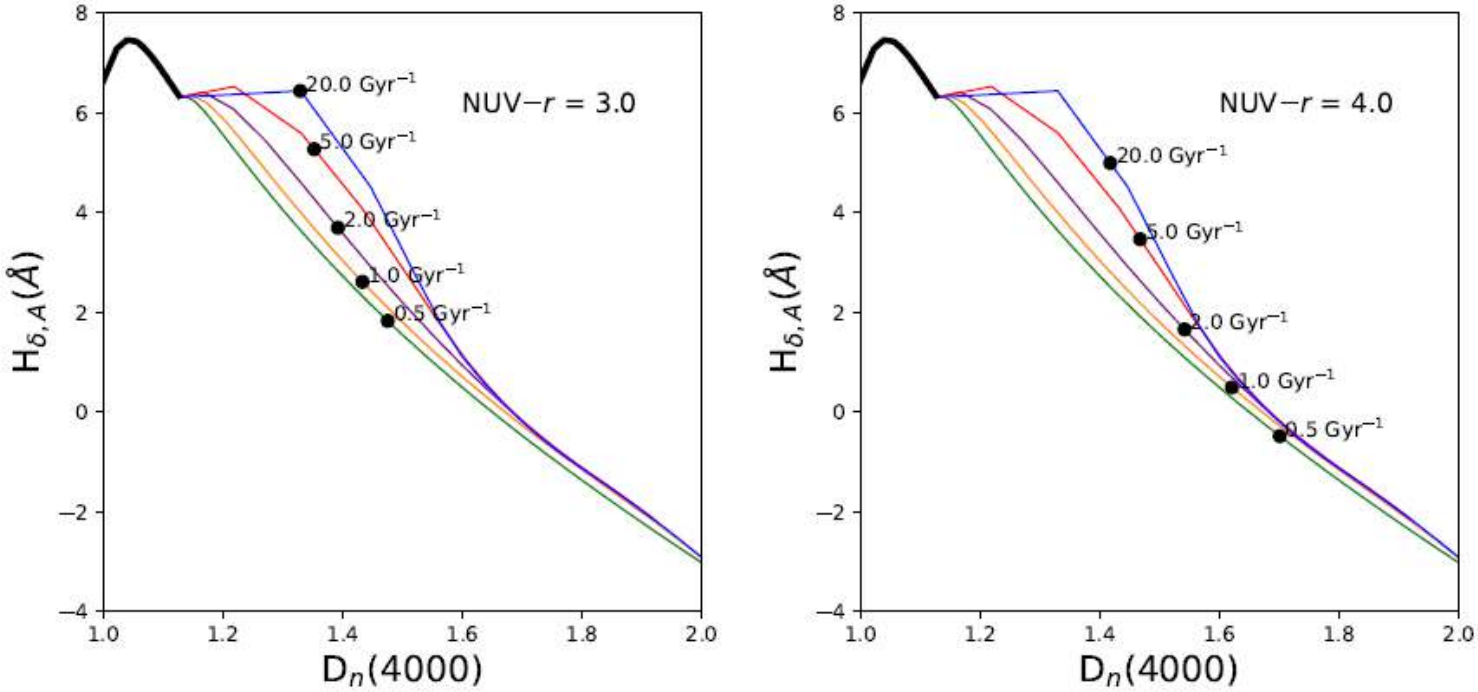

Figure 2. $H_{\delta A} \times D_n(4000)$ planes for the five SFH models shown in Figure 1. The black dots represent the $H_{\delta A}$ and $D_n(4000)$ values for a given SFH model and NUV$-r$ colour. We can see clearly that different NUV$-r$ colours lead to different $H_{\delta A}$ and $D_n(4000)$ values in the same SFH models.

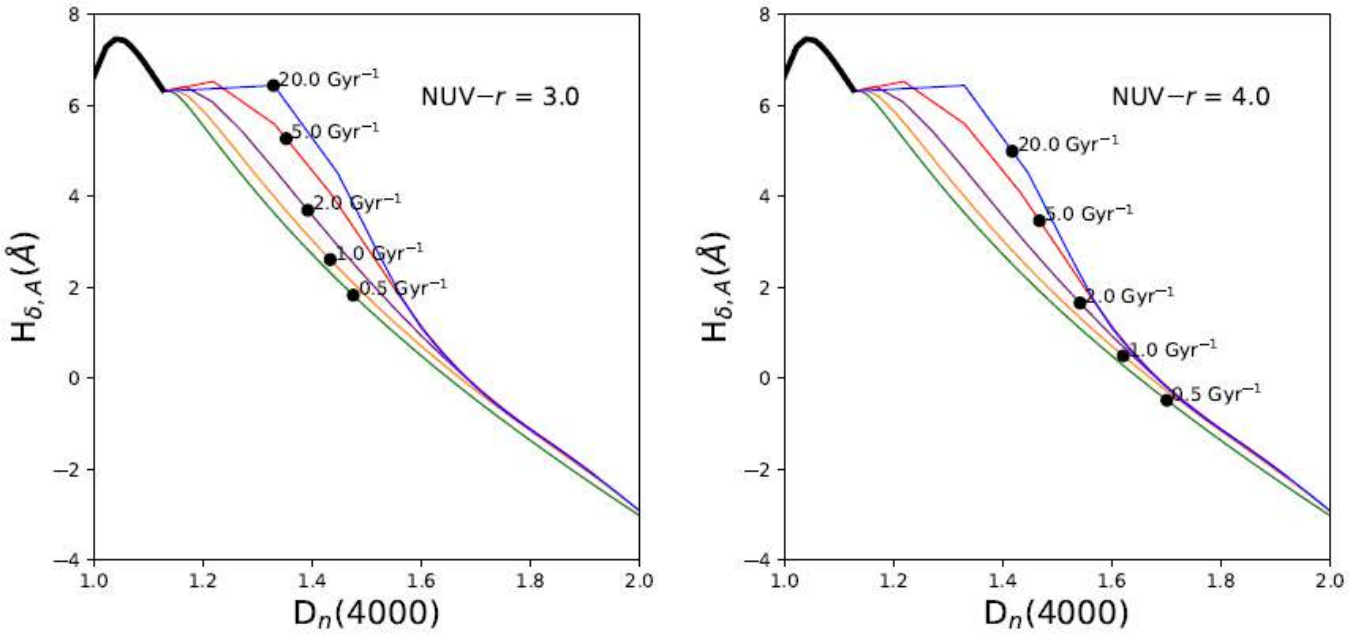

Figure 2. $H_{\delta,A} \times D_n(4000)$ planes for the five SFH models shown in Figure 1. The black dots represent the $H_{\delta,A}$ and $D_n(4000)$ values for a given SFH model and NUV$-r$ colour. We can see clearly that different NUV$-r$ colours lead to different $H_{\delta,A}$ and $D_n(4000)$ values in the same SFH models.

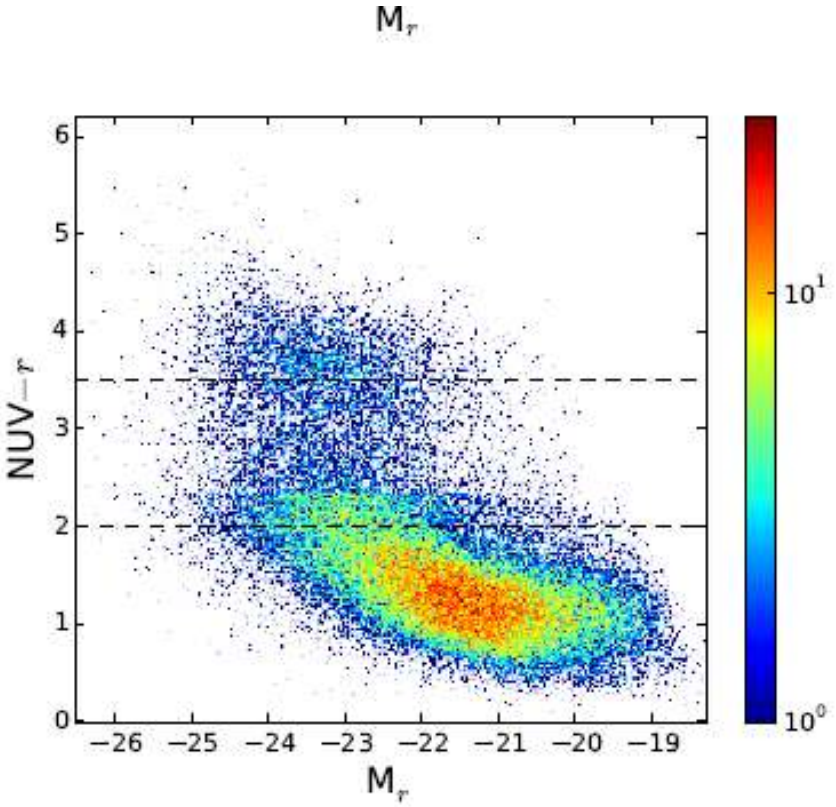

Figure 4. Colour-magnitude diagrams of the Canada-France-Hawaii Telescope Legacy Survey galaxies used in this work. The top panel does not take into account the dust effects whereas the bottom panel is corrected by dust extinction. The horizontal axis represents the Sloan Digital Sky Survey *r*-band absolute magnitude and the vertical axis represents the colour NUV−*r* which can best distinguish the galaxy populations (blue cloud, green valley and red sequence). The dashed horizontal lines delimit the green valley region. The red sequence is not well represented because

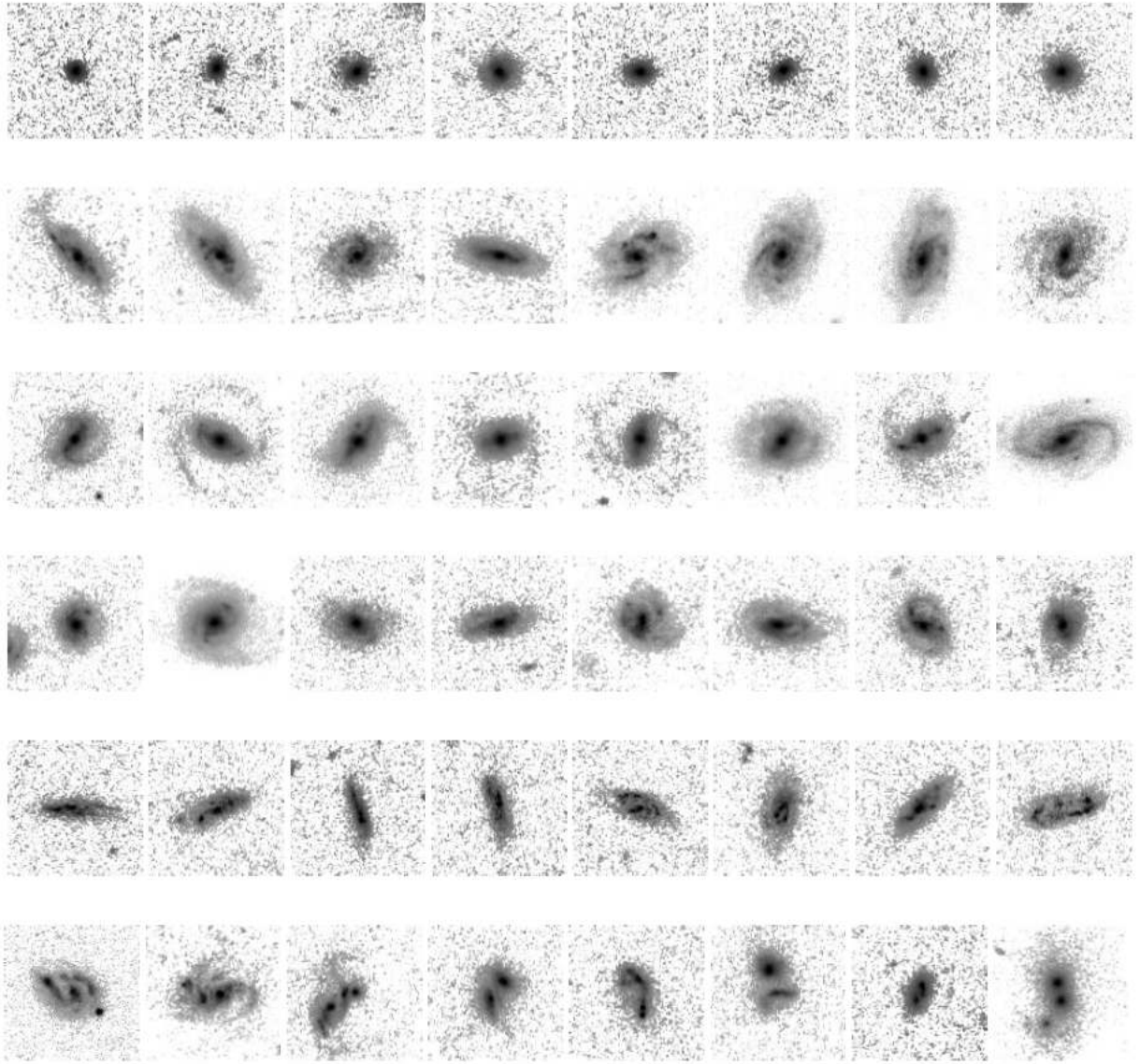

Figure 5. Examples of green valley galaxy images in our sample taken with the Hubble Space Telescope (5" × 5" in size). From the top to the bottom rows these galaxies are classified as ellipticals, unbarred disks, strongly barred disks, weakly barred disks, irregulars and merging galaxies.

Galaxy Type	Number of galaxies	$\langle NUV-r \rangle$	γ [Gyr^{-1}]
Unbarred Disks	94	3.5 ± 0.45	4.17 ± 0.37
Strongly Barred Disks	15	3.4 ± 0.35	1.7 ± 0.24
Weakly Barred Disks	11	3.4 ± 0.23	4.79 ± 0.75
Disks	120	3.5 ± 0.42	3.66 ± 0.2
Ellipticals	108	4.0 ± 0.35	6.08 ± 0.49
Irregulars	48	3.4 ± 0.30	8.97 ± 1.73
Merging	20	3.7 ± 0.50	20.43 ± 3.64

Table 1. Quenching indices and colour values for each galaxy type

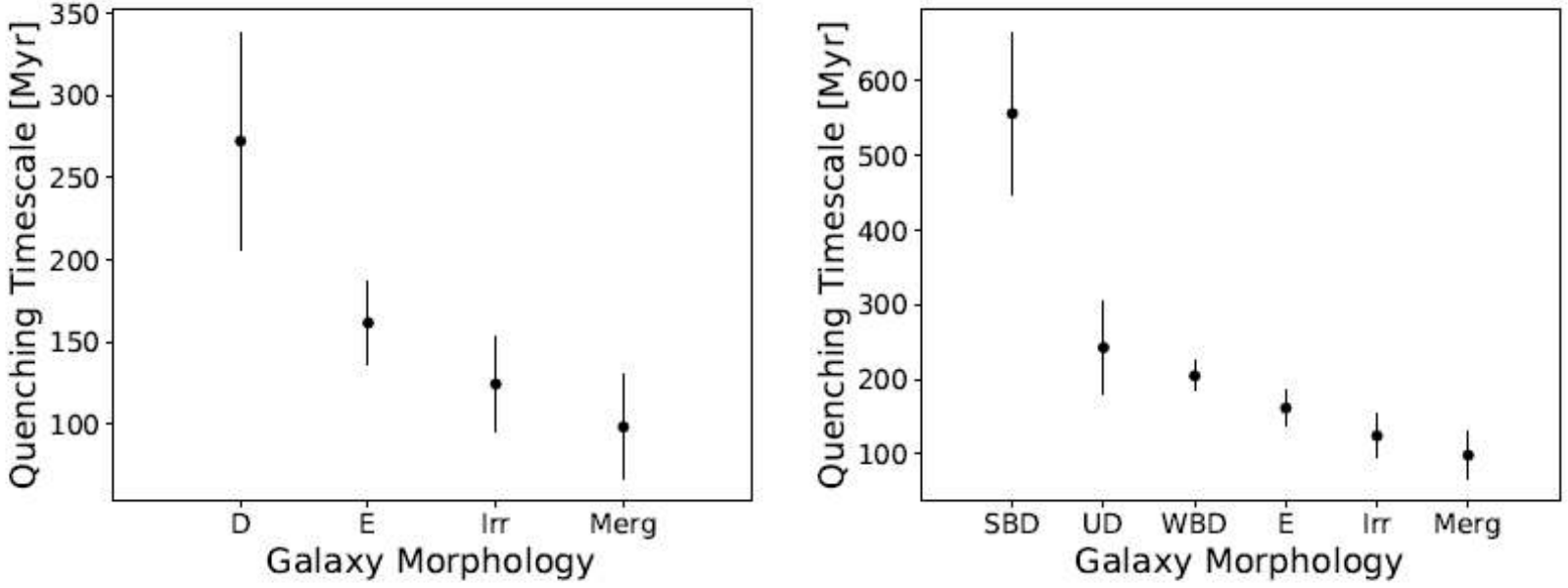

Figure 8. ***Top:*** Quenching index (γ) as a function of galaxy morphology. The left Figure shows the γ values for the green valley galaxies classified as disk (D), ellipticals (E), irregulars (Irr) and merging galaxies (Merg). In the right Figure we divided the disk galaxies into strongly barred disks (SBD), unbarred disks (UD) and weakly barred disks (WBD). ***Bottom:*** Quenching timescales when the initial star formation rate decreases to $\sim$37% of the initial value ($1/\gamma$).

Our analysis of star formation quenching timescales as a function of galaxy morphology at intermediate redshifts (z~0.5 -1) suggests that both secular evolution and merger activity are common processes within the green valley.

However, although secular evolution does appear to play a role in the gas exhaustion in green valley galaxies, the longer timescales associated to barred galaxies relative to those of morphologies reminiscent of merger activity suggests that they are not the main driver of the rapid quenching of galaxies at these redshifts. Galaxy interaction, associated with the elliptical, irregular and merger morphologies contribute, to a more significant degree, to the fast transition through the green valley at these redshifts.

DEEP CO(1-0) OBSERVATIONS OF $Z = 1.62$ CLUSTER GALAXIES WITH SUBSTANTIAL MOLECULAR GAS RESERVOIRS AND NORMAL STAR FORMATION EFFICIENCIES

Gregory Rudnick[1,2,3], Jacqueline Hodge[2,4,5,6], Fabian Walter[2], Ivelina Momcheva[7], Kim-Vy Tran[8], Casey Papovich[8], Elisabete da Cunha[2,10], Roberto Decarli[2], Amelie Saintonge[11], Christopher Willmer[9], Jennifer Lotz[12], Lindley Lentati[13]

ApJ in press

0963v1 [astro-ph.GA] 20 Sep 2017

ABSTRACT

We present an extremely deep CO(1–0) observation of a confirmed $z = 1.62$ galaxy cluster. We detect two spectroscopically confirmed cluster members in CO(1–0) with $S/N > 5$. Both galaxies have $\log(\mathcal{M}_\star/\mathcal{M}_\odot) > 11$ and are gas rich, with $\mathcal{M}_{\rm mol}/(\mathcal{M}_\star+\mathcal{M}_{\rm mol}) \sim 0.17-0.45$. One of these galaxies lies on the star formation rate (SFR)-$\mathcal{M}_\star$ sequence while the other lies an order of magnitude below. We compare the cluster galaxies to other SFR-selected galaxies with CO measurements and find that they have CO luminosities consistent with expectations given their infrared luminosities. We also find that they have comparable gas fractions and star formation efficiencies (SFE) to what is expected from published field galaxy scaling relations. The galaxies are compact in their stellar light distribution, at the extreme end for all high redshift star-forming galaxies. However, their SFE is consistent with other field galaxies at comparable compactness. This is similar to two other sources selected in a blind CO survey of the HDF-N. Despite living in a highly quenched proto-cluster core, the molecular gas properties of these two galaxies, one of which may be in the processes of quenching, appear entirely consistent with field scaling relations between the molecular gas content, stellar mass, star formation rate, and redshift. We speculate that these cluster galaxies cannot have any further substantive gas accretion if they are to become members of the dominant passive population in $z < 1$ clusters.

Subject headings: Galaxies: clusters, Galaxies: evolution, Galaxies: high-redshift, Galaxies: ISM, Galaxies: star formation

1. INTRODUCTION

1.1. *The Evolution of Massive Galaxies*

Understanding the regulation and demise of star formation in the most massive ($\log(\mathcal{M}_\star/\mathcal{M}_\odot) \gtrsim 11$) galaxies is a dominant theme of galaxy evolution studies. An important epoch for understanding the evolution in this population is $1 < z < 2$. This epoch was roughly 50% of $\log(\mathcal{M}_\star/\mathcal{M}_\odot) > 11$ galaxies were in place (e.g. Dickinson et al. 2003; Rudnick et al. 2003; Fontana et al. 2003; Rudnick et al. 2006; Fontana et al. 2006; Pozzetti et al. 2007; Marchesini et al. 2009; Ilbert et al. 2010; van Dokkum et al. 2010).

Large surveys of representative volumes in the local Universe, such as SDSS, have determined that the mas-

1709.06963

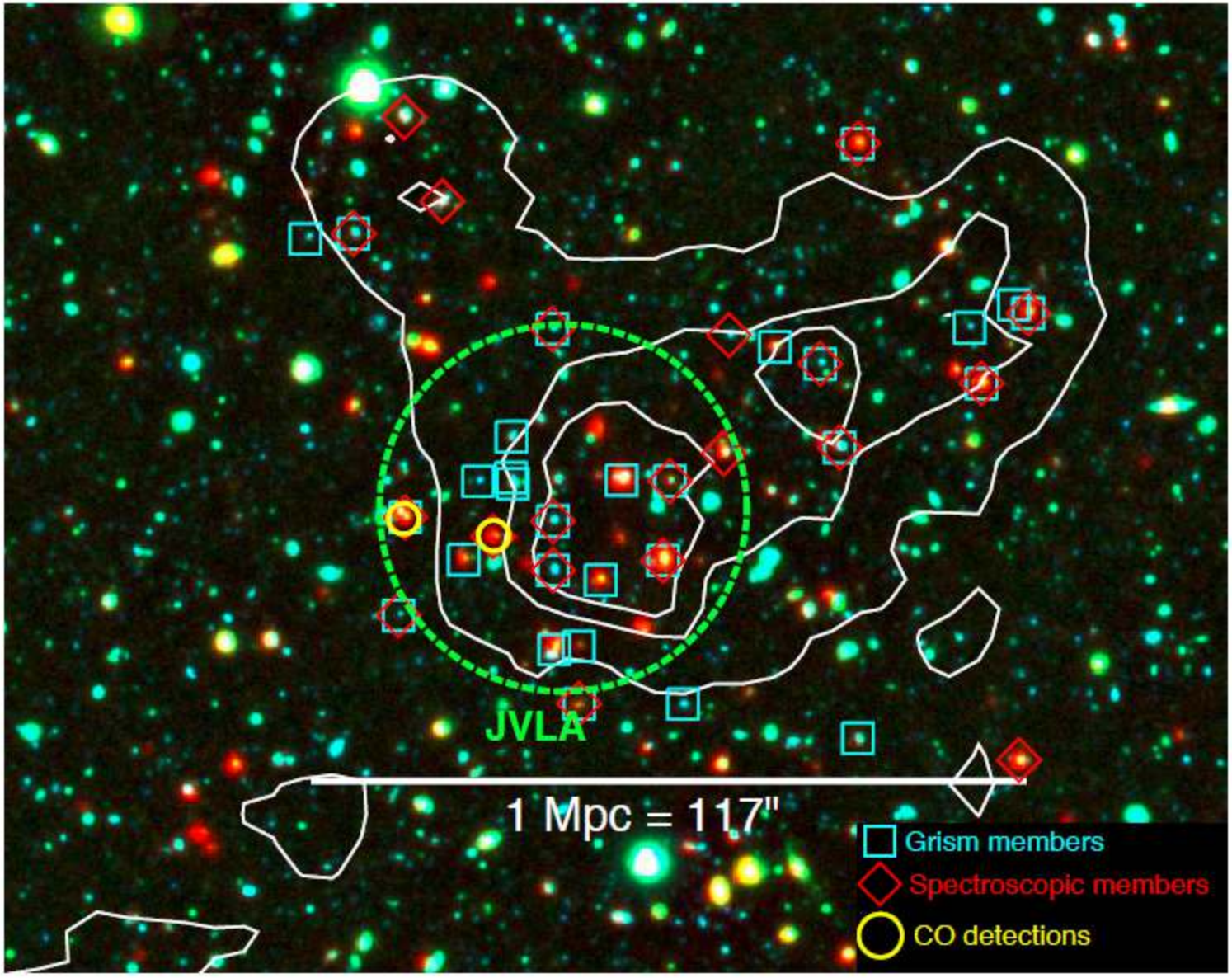

Figure 1. A $Bi[4.5\mu m]$ image of XMM-LSS J02182-05102. The contours denote regions with 5, 10, and 15σ above the mean density galaxies with $1.5 < z_{phot} < 1.7$ from the UKIDSS UDS K-selected catalog presented in Papovich et al. (2010). The green dashed cir illustrates our pointing of the VLA, with the size of the circle corresponding to the FWHM of the beam at 43.913 GHz. The yellow circ indicate the two CO(1–0) detections. The red diamonds mark all spectroscopically confirmed members and the cyan squares mark

Table 1
Stellar Population Parameters of CO-detected Galaxies

ID	$\log(\mathcal{M}_*/\mathcal{M}_\odot)$[a]	SFR[a] $[\mathcal{M}_\odot\ \mathrm{yr}^{-1}]$	$\log(\mathrm{L}_{IR}/L_\odot)$[a]	$r_{1/2}$[b] [kpc]	n[c]	q[d]
30169	$11.22^{+0.15}_{-0.15}$	$12.0^{+7.5}_{-3.5}$	$11.46^{+0.15}_{-0.15}$	4.15 ± 0.17	0.6 ± 0.1	0.23 ± 0.03
30545[e]	$11.14^{+0.15}_{-0.15}$	$155.6^{+64.2}_{-45.4}$	$12.23^{+0.15}_{-0.15}$	1.93 ± 0.15	2.7 ± 0.4	0.76 ± 0.05

[a] Computed from the MAGPHYS (da Cunha et al. 2008) fits to the full SED from the u-band through the *Herschel* SPIRE bands at 500μm. We assign a minimum 0.15 dex uncertainty to all quantities.
[b] The effective radius for a Sérsic (1968) fit to the F160W HST/WFC3 imaging from van der Wel et al. (2012).
[c] The Sérsic (1968) index of the fit to the F160W HST/WFC3 imaging from van der Wel et al. (2012).
[d] The minor-to-major axis ration of the fit to the F160W HST/WFC3 imaging from van der Wel et al. (2012).
[e] The observed optical and NIR photometry for this source are well separated from the neighbor 30577. It is possible that the MIPS 24μm and Herschel fluxes may include contributions from 30545 and the neighbor 30577. As the SFR is dominated by the FIR emission for the Herschel source, if it is blended we should still be measuring the total SFR corresponding to the CO detection.

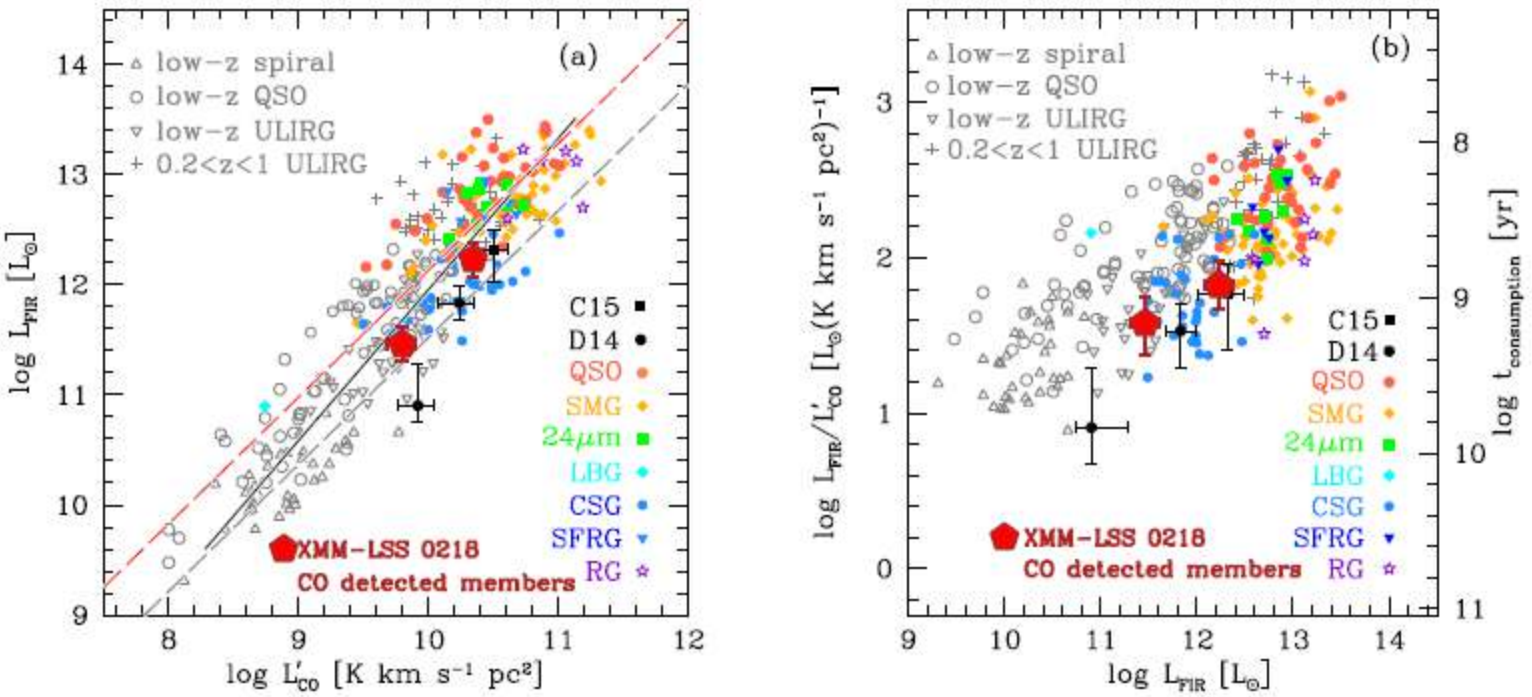

Figure 7. *Left Panel:* A comparison of the infrared luminosities and CO luminosities of our two CO detected cluster members at $z = 1.625$ (large filled Pentagons) with a sample of star-forming galaxies and QSOs over a wide range of redshift taken from Carilli & Walter (2013) and which includes various local galaxies as well as all systems detected in CO at $z > 1$ as of 2013. In addition, we show two galaxies from D14 that were detected in a blind CO survey of the HDF-N and one from Chapman et al. (2015, C15) that was detected in a blind survey of a proto-cluster at $z = 2.3$. L_{IR} is a proxy for the SFR and the L'_{CO} is a proxy for the gas mass, modulo α_{CO}. The solid line is a fit to all data points, which gives a slope of 1.35 ± 0.04. The dashed lines indicate the best fits for the main sequence galaxies (gray) and starburst galaxies (red) derived by Genzel et al. (2010) and Daddi et al. (2010a). *Right Panel:* We compare the ratio of L_{IR}/L'_{CO} to L_{IR} for the same galaxies as shown in the left-hand panel. L_{IR}/L'_{CO} is a proxy for SFR/$\mathcal{M}_{\rm mol}$ or the star formation efficiency. On the right axis we plot the consumption timescale. Our two cluster members are forming stars with typical SFE and have $t_{\rm con}$ similar to other gas-rich galaxies at their L_{IR}. The legend abbreviations in both plots stand for: QSO – quasi-stellar objects; SMG – submillimeter galaxies; 24μm– sources selected by 24μm flux; LBG – Lyman Break galaxies; CSG – rest-frame UV color-selected "BM/BX" galaxies; SFRG – star-forming radio galaxies; RG – radio galaxies.

5.1. α_{CO} *and the nature of high redshift star formation*

The foremost uncertainty is the value for α_{CO}, which determines the conversion of L'_{CO} to $\mathcal{M}_{\rm mol}$. We adopt a Galactic value of α_{CO}=4.36 and show that it is broadly consistent with our limited dynamical constraints, although an α_{CO} that is lower by 50% may be appropriate for 30545 to avoid having the baryonic mass for 30545 in excess of the dynamical mass (see §3.5). If a ULIRG-like α_{CO}=0.8 is more appropriate, it would reduce our gas masses by a factor of ~ 5 and make our SFEs more consistent with other star-forming galaxies at these redshifts.

Our galaxies lie in a forming cluster and studies of the likely descendant clusters at $z < 1$ indicate that our galaxies have a high probability of becoming passive in the intervening 1.8 Gyr between $z = 1.62$ and 1. If that is their destiny, then to become passive, and presumably gas poor, by $z = 1$ means that our galaxies cannot tolerate any further gas accretion following the epoch in which we observe them. This might indicate that galaxies in the forming cluster environment have been decoupled from their gas umbilical cords that connect them to the cosmic web and may be the early manifestation of the process known variously as starvation or strangulation.

A method to calculate the local density distribution of the Galaxy from the Tycho-Gaia Astrometric Solution data

Rain Kipper[1]★, Elmo Tempel[1,2] and Peeter Tenjes[1]
[1]*Tartu Observatory, Observatooriumi 1, 61602 Tõravere, Estonia*
[2]*Leibniz-Institut für Astrophysik Potsdam (AIP), An der Sternwarte 16, 14482 Potsdam, Germany*

:1709.06744v1 [astro-ph.GA] 20 Sep 2017

Accepted 2017 September 19. Received 2017 September 19; in original form 2017 June 29

ABSTRACT

New and more reliable distances and proper motions of a large number of stars in the Tycho-Gaia Astrometric Solution (TGAS) catalogue allow to calculate the local matter density distribution more precisely than earlier.

We devised a method to calculate the stationary gravitational potential distribution perpendicular to the Galactic plane by comparing the vertical probability density distribution of a sample of observed stars with the theoretical probability density distribution computed from their vertical coordinates and velocities. We applied the model to idealised test stars and to the real observational samples. Tests with two mock datasets proved that the method is viable and provides reasonable results.

Applying the method to TGAS data we derived that the total matter density in the Solar neighbourhood is 0.09 ± 0.02 $M_\odot pc^{-3}$ being consistent with the results from literature. The matter surface density within $|z| \leq 0.75$ kpc is 42 ± 4 $M_\odot pc^{-2}$. This is slightly less than the results derived by other authors but within errors is consistent with previous estimates. Our results show no firm evidence for significant amount of dark matter in the Solar neighbourhood. However, we caution that our calculations at $|z| \leq 0.75$ kpc rel on an extrapolation from the velocity distribution function calculated at $|z| \leq 25$ pc. This extrapolation can be very sensitive to our assumption that the stellar motions are perfectly decoupled in R and z, and to our assumption of equilibrium. Indeed, we find that $\rho(z)$ within $|z| \leq 0.75$ kpc is asymmetric with respect to the Galactic plane at distances $|z| = 0.1 - 0.4$ kpc indicating that the density distribution may be influenced by density perturbations.

Key words: Galaxy: fundamental parameters – Galaxy: kinematics and dynamics – Solar neighbourhood – stars: kinematics and dynamics – methods: data analysis

1 INTRODUCTION

having certain constraints to its value it is possible to esti-

Derived local spatial matter density value $\rho_0 = 0.09 \pm 0.02\ \mathrm{M_\odot pc^{-3}}$ is only slightly larger than the estimated sum of the stellar and gas mass densities $\rho_0 = 0.084 \pm 0.012\ \mathrm{M_\odot pc^{-3}}$ (McKee et al. 2015). Thus, the local density of dark matter is rather small $\rho_{\mathrm{DM}} = 0.006\ \mathrm{M_\odot pc^{-3}}$. Taking into account 2σ errors the local dark matter density would be $\leq 0.038\ \mathrm{M_\odot pc^{-3}}$.

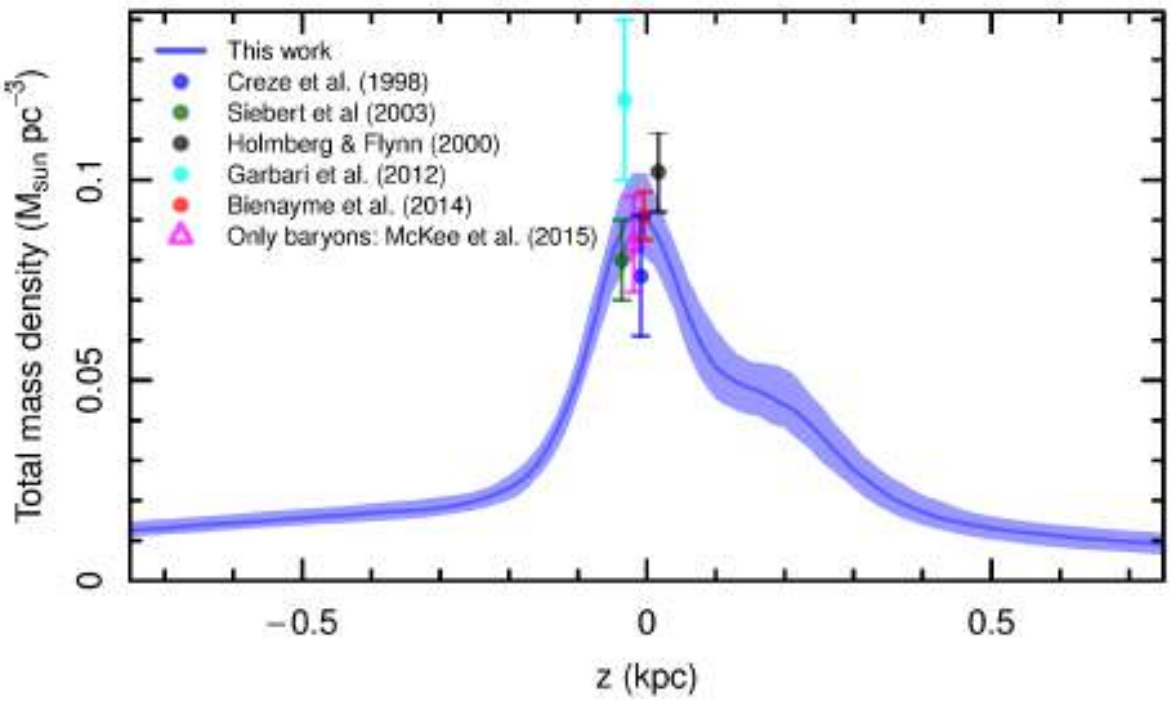

Figure 11. Calculated total matter density distribution of the model. The blue region denotes our one sigma posterior distribution of the density corresponding to the MCMC points. This contains only statistical errors of the fitting and not errors from observational uncertainties. Density values at $z = 0$ derived by other authors are given by coloured filled circles.

It is seen from Fig. 11 that the density distribution is asymmetric with respect to the Galactic plane. The asymmetry is twofold. First, disc plane has a small offset by about $0.01-0.02$ kpc and second, the densities at positive z values up to $z \sim 0.4$ kpc are systematically larger than those at corresponding negative values.